REGULAR ARTICLE

blood advances

An inducible *Cd79b* mutation confers ibrutinib sensitivity in mouse models of *Myd88*-driven diffuse large B-cell lymphoma

Ruth Flümann,[1-5,*] Julia Hansen,[1,5,*] Jörn Meinel,[6] Pauline Pfeiffer,[1] Hannah Goldfarb Wittkopf,[1,5] Anna Lütz,[1,5] Jessica Wirtz,[1,5] Michael Möllmann,[7] Tanja Zhou,[7] Areya Tabatabai,[7] Tim Lohmann,[1] Maximilian Jauch,[7] Filippo Beleggia,[1,4,8] Benedikt Pelzer,[9] Fabian Ullrich,[7] Svenja Höfmann,[7] Aastha Arora,[7] Thorsten Persigehl,[10] Reinhard Büttner,[6] Bastian von Tresckow,[7] Sebastian Klein,[7,*] Ron D. Jachimowicz,[1-5,*] Hans Christian Reinhardt,[7,*] and Gero Knittel[7,*]

[1]Department I of Internal Medicine, Center for Integrated Oncology Aachen Bonn Cologne Düsseldorf, Faculty of Medicine and University Hospital Cologne, University of Cologne, Cologne, Germany; [2]Center for Molecular Medicine, and [3]Cologne Excellence Cluster on Cellular Stress Response in Aging-Associated Diseases, University of Cologne, Cologne, Germany; [4]Mildred Scheel School of Oncology Aachen Bonn Cologne Düsseldorf, Faculty of Medicine and University Hospital of Cologne, Cologne, Germany; [5]Max Planck Institute for Biology of Ageing, Cologne, Germany; [6]Institute of Pathology, Faculty of Medicine and University Hospital Cologne, University of Cologne, Cologne, Germany; [7]Department of Hematology and Stem Cell Transplantation, West German Cancer Center, German Cancer Consortium Partner Site Essen, Center for Molecular Biotechnology, University Hospital Essen, University of Duisburg-Essen, Essen, Germany; [8]Department of Translational Genomics, Faculty of Medicine and University Hospital Cologne, University of Cologne, Cologne, Germany; [9]Division of Hematology/Oncology, Department of Medicine, Weill Cornell Medicine, Cornell University, New York, NY; and [10]Department of Radiology and Interventional Radiology, Faculty of Medicine and University Hospital Cologne, University of Cologne, Cologne, Germany

Key Points

- In mouse models of *Myd88*-driven DLBCL, the presence of a *Cd79b* ITAM mutation results in increased B-cell receptor proximal signaling.
- The increased B-cell receptor signaling activity in *Cd79b*-mutated models confers a selective ibrutinib sensitivity.

Diffuse large B-cell lymphoma (DLBCL) is the most common aggressive lymphoma and constitutes a highly heterogenous disease. Recent comprehensive genomic profiling revealed the identity of numerous molecularly defined DLBCL subtypes, including a cluster which is characterized by recurrent aberrations in *MYD88*, *CD79B*, and *BCL2*, as well as various lesions promoting a block in plasma cell differentiation, including *PRDM1*, *TBL1XR1*, and *SPIB*. Here, we generated a series of autochthonous mouse models to mimic this DLBCL cluster and specifically focused on the impact of *Cd79b* mutations in this setting. We show that canonical *Cd79b* immunoreceptor tyrosine-based activation motif (ITAM) mutations do not accelerate *Myd88*- and *BCL2*-driven lymphomagenesis. *Cd79b*-mutant murine DLBCL were enriched for IgM surface expression, reminiscent of their human counterparts. Moreover, *Cd79b*-mutant lymphomas displayed a robust formation of cytoplasmic signaling complexes involving MYD88, CD79B, MALT1, and BTK. These complexes were disrupted upon pharmacological BTK inhibition. The BTK inhibitor–mediated disruption of these signaling complexes translated into a selective ibrutinib sensitivity of lymphomas harboring combined *Cd79b* and *Myd88* mutations. Altogether, this in-depth cross-species comparison provides a framework for the development of molecularly targeted therapeutic intervention strategies in DLBCL.

Submitted 14 July 2023; accepted 26 November 2023; prepublished online on *Blood Advances* First Edition 7 December 2023; final version published online 28 February 2024. https://doi.org/10.1182/bloodadvances.2023011213.

*R.F., J.H., S.K., R.D.J., H.C.R., and G.K. contributed equally to this study.

Murine exomes, transcriptomes, and B-cell receptor sequencing data are available at the European Nucleotide Archive (accession number PRJEB69524).

Data are currently being uploaded and will be available within the next days. Data are available to the reviewers upon request from the corresponding author, H. C. Reinhardt (christian.reinhardt@uk-essen.de).

The full-text version of this article contains a data supplement.

Introduction

Diffuse large B-cell lymphoma (DLBCL) is the most common lymphoid malignancy in adults, accounting for ~35% of B-cell non-Hodgkin lymphomas.[1] DLBCL is a heterogeneous disease that has traditionally been subdivided into germinal center B-cell–like (GCB) and activated B-cell–like (ABC) DLBCL, based on transcriptome profiling.[2] This cell of origin–based stratification separates DLBCL subtypes displaying distinct pathogenesis and response to anthracycline-based firstline chemoimmune therapy.[3-5]

Recently, comprehensive genomic profiling led to the discovery of partially overlapping genetic DLBCL subtypes.[6,7] These clusters were defined by: (1) *BCL6* structural variants co-occurring with *NOTCH2* aberrations (C1); (2) biallelic deleterious *TP53* aberrations (*TP53* mutations and 17p copy number alterations) together with haploinsufficiencies of *CDKN2A* and *RB1* (C2); (3) *BCL2* mutations together with *BCL2* structural variants in combination with *EZH2*, *CREBBP*, and *KMT2D* mutations and additional activating alterations affecting the PI3K pathway (C3); (4) mutations in histone genes together with aberrations in immune evasion molecules, NF-κB, and RAS/JAK/STAT signaling molecules (C4); and (5) 18q copy number gains, likely affecting *BCL2*, with concurrent *MYD88* and *CD79B* mutations (C5).[6] A separate analysis defined 4 clusters, namely cases with *BCL6* rearrangements and *NOTCH2* mutations (BN2), *EZH2* mutations and *BCL2* rearrangements (EZB), *NOTCH1* mutations (N1), as well as co-occurring *MYD88* and *CD79B* mutations (MCD).[7] With respect to clinical applicability, it is important to note that these clusters could, in large parts, be recapitulated by applying clustering techniques to targeted sequencing data obtained from a large, unselected population-based patient cohort.[8] To further facilitate clinical applicability of genetic clustering of DLBCL cases, the LymphGen algorithm was established, which enables a probabilistic classification-based approach to bin a tumor from an individual patient into a genetic subtype.[9] This algorithm builds on the NCI and Harvard genomic data sets[6,7] and subdivides DLBCL into 7 molecularly defined subtypes.[9]

Therapeutically, frontline chemoimmune therapy using R-CHOP or similar regimens achieves cure rates of ~65% in DLBCL.[6,10-12] However, relapsed or refractory (R/R) disease represents a major clinical challenge, because these patients are typically difficult to salvage, and even high-dose chemotherapy regimens followed by autologous stem cell transplantation, chimeric antigen receptor T-cell therapies, or bispecific antibodies, frequently, do not provide long-term disease control.[13-17] Thus, the development and preclinical validation of treatment strategies for R/R DLBCL and less toxic treatment options for older and frail patients are urgently needed.

We previously reported the generation of mouse models of *Myd88*-driven DLBCL.[18-20] These models were constructed through the combination of B-cell–specific expression of oncogenic *Myd88* and *BCL2* together with the deletion of *Prdm1* or overexpression of *Spib*. Although these models, specifically the $Cd19^{Cre/wt}$;$Myd88^{c.\cdot p.L252P/wt}$;$Rosa26^{LSL.BCL2.IRES.GFP/wt}$;$Prdm1^{fl/fl}$ model, captured central transcriptomic and surface marker features of C5/MCD DLBCL, they lacked co-occurring *Cd79b* mutations, which significantly cocluster with *MYD88* p.L265P in human C5 DLBCL.[6] *CD79B* mutations in human DLBCL typically affect the first tyrosine residue within the immunoreceptor tyrosine-based activation motif (ITAM) through amino acid substitutions or deletions of this residue or sometimes deletions or partial deletions of the entire ITAM.[3,6,7] Importantly, ABC-DLBCLs typically retain at least 1 intact ITAM in either *CD79A* or *B*, likely to serve as a signaling adaptor for SYK and other B-cell receptor (BCR) signaling effector molecules.[3,6,7] It is also noteworthy that *CD79B* depletion is toxic in ABC-DLBCL cell lines.[21] Here, we set out to engineer a B-cell–specific inducible mutation of the first ITAM tyrosine residue and assess the biological function of this mutation on our various C5/MCD DLBCL mouse models.

Methods

Experimental animals

The generation of the $Myd88^{cond.p.L252P}$ and $Rosa26^{LSL.BCL2\text{-}IRES\text{-}GFP}$ alleles has been described previously.[18-20] The $Prdm1^{flox}$ and $Cd19^{Cre}$ alleles were purchased from The Jackson Laboratory.[22,23]

Generation of the $Cd79b^{c\text{-}p.Y195H}$ allele: The targeting vector depicted in supplemental Figure 1A, was generated using standard techniques. The *Cd79b* wildtype sequence was based on the NCBI transcript NM_008339.2. Wildtype exons 3 to 6 were flanked by loxP sites. A polyadenylation signal (hGHpA) was inserted between the 3' UTR and the distal loxP site. Downstream of the distal loxP site, copies of exons 3 to 6 harboring the p.Y195H mutation were inserted. Furthermore, a FRT-site flanked neomycin resistance cassette and an F3-flanked puromycin resistance cassette were inserted into the targeting vector, which was then electroporated into C57BL/6NTac embryonic stem cells. Positive clones were derived by dual selection with G418 and puromycin. Correct integration was verified by Southern blotting before blastocyst injection. Germ line–transmitting founder animals were received and crossbred with a FlpDel line to remove the puromycin and neomycin resistance cassettes. To record survival, an event was registered when either the animal succumbed to disease or had to be euthanized due to the predefined humane termination criteria. Animals that died of or had to be euthanized because of genotype-unspecific reasons were censored. These unrelated reasons included abnormal teeth and injuries inflicted by cage mates.

Treatment studies were performed as described previously.[18] In brief, animals were defined as lymphoma-bearing as soon as a lesion >150 μL or splenomegaly >500 μL and a robust volume increase were detectable by magnetic resonance imaging (MRI) in 2 consecutive scans. After lymphoma diagnosis, ibrutinib (MedChem Tronica) was administered daily by oral gavage for 3 weeks as a suspension in 0.4% methylcellulose at 30 mg/kg body weight, then via drinking water until death. Drinking water was prepared by dissolving ibrutinib in 5% HP-Cyclodextrin (PanReac Applichem) at 0.16 mg/mL. Mice could drink ibrutinib drinking water ad libitum with no other source of water, receiving ~30 mg/kg body weight ibrutinib per day.[24] For samples collected from acutely treated mice, ibrutinib was administered daily by oral gavage for 3 days at 30 mg/kg body weight, and then mice were euthanized for sample collection on the fourth day.

MRI was performed as previously described.[19,25,26]

All animals were housed in a specific-pathogen-free facility, and experiments were approved by the local animal care committee and the relevant authorities (Landesamt für Natur, Umwelt und Verbraucherschutz Nordrhein-Westfalen, AZ: 84-02.04.2017.A131, 84-02.04.2014.A146, 81-02.04.2019.A009).

Results

Generation of a mouse model that faithfully recapitulates *MYD88/CD79B*-mutant DLBCL

We previously described murine models of human C5/MCD DLBCL that are driven by B-cell–specific expression of *Myd88*$^{p.L252P}$ (*Myd88*$^{c.-p.L252P}$ [M], orthologous position of the human *MYD88*$^{p.L265P}$ mutation), conditional overexpression of *BCL2* from the *Rosa26* locus (*Rosa26*$^{LSL.BCL2.IRES.GFP}$ [B]), and homozygous deletion of *Prdm1* (*Prdm1*$^{fl/fl}$ [PP]).[18-20] B-cell specificity was achieved through the use of a *Cd19*^{Cre} allele (C).

Here, we generated a conditional *Cd79b*$^{p.Y195H}$ allele (*Cd79b*$^{c.-p.Y195H}$ [79]) that is expressed from the endogenous locus upon Cre-mediated recombination (Figure 1A and supplemental Figure 1A). Murine *Cd79b*$^{p.Y195H}$ is at the orthologous position of the first tyrosine residue of the human *CD79B* ITAM. To verify Cre-inducible *Cd79b*$^{p.Y195H}$ expression, we generated germ line–recombined *Cd79b*$^{p.Y195H/p.Y195H}$ and *Cd79b*$^{wt/wt}$ control mice. Using Sanger sequencing, we detected the expression of *Cd79b*^{wt} messenger RNA in B cells derived from *Cd79b*$^{wt/wt}$, whereas only *Cd79b*$^{p.Y195H}$-mutant messenger RNA was detected in *Cd79b*$^{p.Y195H/p.Y195H}$-derived B cells (supplemental Figure 1B). CD79B surface expression, assessed by flow cytometry, was unaffected in *Cd79b*$^{p.Y195H/p.Y195H}$ B cells, indicating that the CD79B$^{p.Y195H}$ isoform is expressed at endogenous levels (supplemental Figure 1C).

To assess the effects of introducing a B-cell–specific *Cd79b* ITAM mutation into the MBC and PPMBC models,[18-20] we generated 79-MBC and 79-PPMBC mice. These animals were born at expected Mendelian ratios and displayed an overall survival (OS) that was indistinguishable from the MBC and PPMBC parental strains (Figure 1A-B). Reminiscent of the MBC and PPMBC parental strains, 79-MBC and 79-PPMBC mice developed life-limiting lymphomas (Figure 1C-E). Engineering of the *Cd79b*$^{c.-p.Y195H}$ allele into the MBC and PPMBC backgrounds did not alter the B220 or CD138 expression patterns or the Ki67 indices, compared with that of the parental strains (Figure 1D-F). We detected minute differences in the infiltration patterns of nodal and extranodal sites between MBC and 79-MBC lymphomas (supplemental Figure 1D). A reduced fraction of 79-MBC animals displayed infiltration of abdominal lymph nodes, compared with MBC mice (supplemental Figure 1E). Furthermore, fewer 79-PPMBC mice displayed submandibular lymph node infiltration than PPMBC mice (supplemental Figure 1E). MBC, 79-MBC, PPMBC, and 79-PPMBC lymphomas were typically dominated by a single large clone with related subclones, likely indicating ongoing somatic hypermutation (Figure 1G-H).

Although MBC, 79-MBC, and PPMBC-derived lymphomas were dominated by immunoglobulin G (IgG) and IgA class-switched BCRs, 79-PPMBC–derived lymphomas mainly expressed IgM BCRs (Figure 1I). This is in line with recently reported data indicating that ABC-DLBCL cases are enriched for IgM BCR using a specific set of V_H genes with reactivity against self antigens.[27] Further corroborating observations were made in human DLBCL, in which ABC-DLBCL cases, which are enriched for MCD/C5 cases,[6,7] typically retain IgM surface expression, whereas GCB DLBCLs rather display IgG BCRs.[28]

Altogether, engineering a B-cell–specific *Cd79b*$^{p.Y195H}$ mutation onto the lymphoma-prone MBC and PPMBC backgrounds led to the development of clonal DLBCL that was morphologically indistinguishable from disease developing in the parental MBC and PPMBC strains. In addition, the *Cd79b* p.Y195H mutation did not increase the fraction of proliferating lymphoma cells, nor did it enhance disease kinetics. We did, however, detect a shift toward IgM surface BCR expression in 79-PPMBC–derived lymphomas, compared with that in PPMBC tumors.

Myd88 and *Cd79b* comutant murine lymphomas display transcriptomic features similar to human ABC-DLBCL

We next performed bulk RNA-sequencing on isolated lymphoma tissue derived from the 4 distinct genotypes. As shown in Figure 2A, unsupervised clustering using a Partitioning Around Medoids approach revealed that particularly loss of *Prdm1* dictated the transcriptome-defined segregation between the 4 lymphoma genotypes, in which MBC and 79-MBC lymphomas were clearly distinct from PPMBC and 79-PPMBC cases. Using this Partitioning Around Medoids approach, we identified 2 clusters (Figures 2A and supplemental Figure 2A), in which cluster 1 was defined by genes overexpressed in PPMBC and 79-PPMBC cases compared to MBC and 79-MBC lymphomas. Cluster 2 contained genes that were overexpressed in MBC and 79-MBC, compared to PPMBC and 79-PPMBC samples (Figure 2A). To uncover gene sets that were associated with each cluster, we applied an overrepresentation analysis, using enrichr.[30] In line with our previously published data,[18] this overrepresentation analysis revealed that PPMBC and 79-PPMBC lymphomas displayed a significantly higher expression of genes associated with the "BCR Signaling Pathway," "TNF-alpha Signaling via NF-κB," "NF-kappaB complex," and "B cell receptor complex" gene sets from the Jensen, Hallmark, and WikiPathways reference gene sets, respectively (Figure 2A).[31-33]

We next deployed the gene expression profiles derived from our 4 distinct lymphoma genotypes to assess their similarity to gene sets derived from a single-cell transcriptome data set that was generated to characterize the distinct human GC B-cell populations.[34] Reminiscent of the data shown in Figure 2A, unsupervised clustering of these data showed that particularly MBC and 79-MBC lymphomas cluster distinctly from PPMBC and 79-PPMBC cases (Figure 2B). This analysis further revealed that MBC and 79-MBC lymphomas showed significantly higher single sample GSEA scores for gene sets associated with late light-zone and plasmablast (PB) stages (supplemental Figure 2B), whereas PPMBC and 79-PPMBC lymphomas were significantly enriched for early light-zone and intermediate stages (supplemental Figure 2B). Moreover, PPMBC and 79-PPMBC lymphomas were significantly enriched for the pre–memory B-cell (MB) gene signature, compared with that of MBC and 79-MBC cases (supplemental Figure 2B). Enrichment analysis of a gene set collection on cellular differentiation ("Staudt cellular differentiation B cell", https://lymphochip.nih.gov/signature.db/) recapitulates an

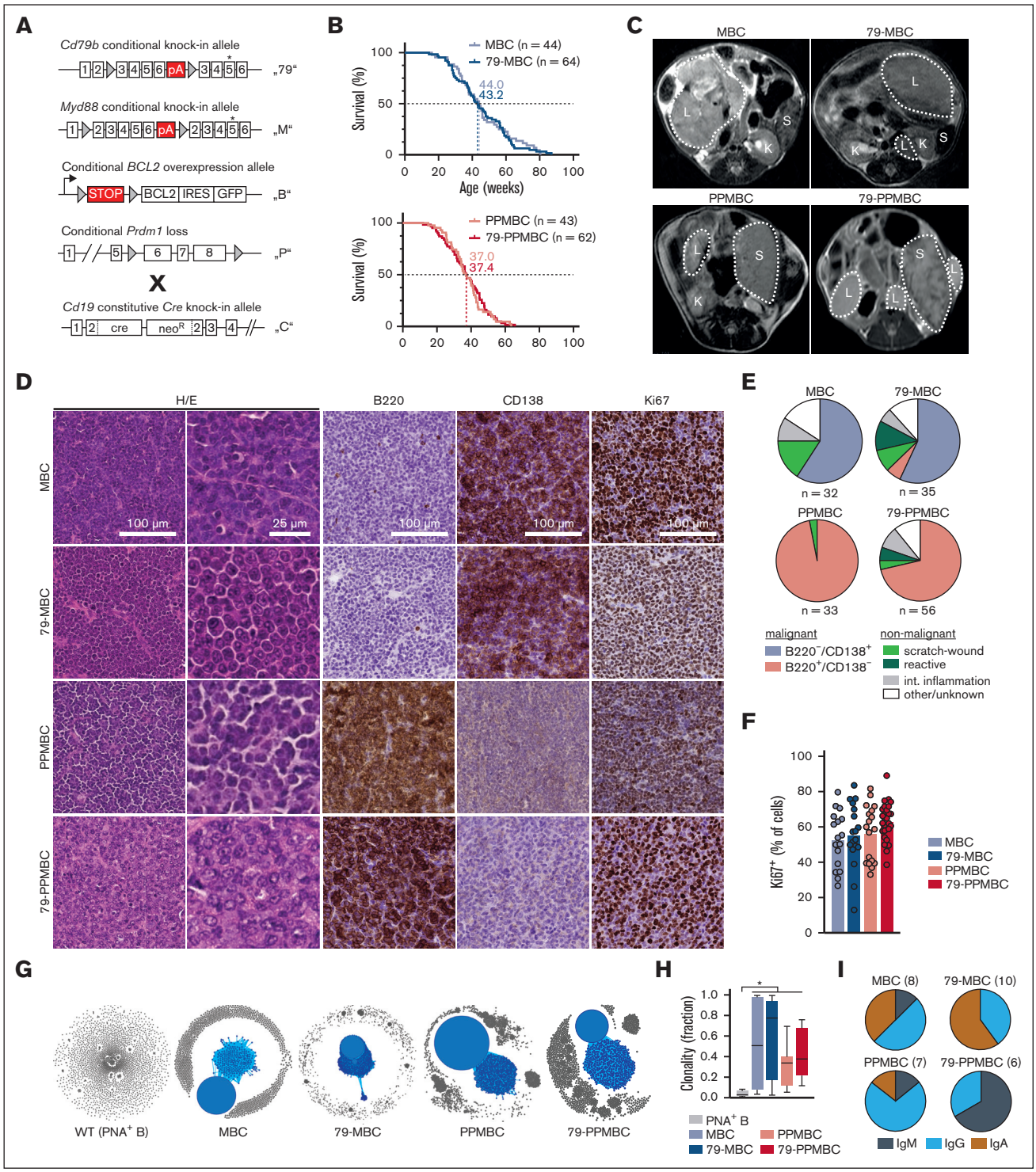

Figure 1. Mouse models develop clonal DLBCL-like disease. (A) Schematic visualizations of the alleles used throughout the manuscript. Triangular shapes represent loxP sites. (B) Survival was determined for both the *Prdm1*-proficient (MBC/79-MBC) and *Prdm1*-deficient (PPMBC/79-PPMBC) models. (C) Representative MRI images of overt lymphoma in the 4 mouse lines; L, lymphoma; S, spleen; and K, kidney. (D) Representative immunohistochemical stainings of lymphoma tissue isolated from MBC, 79-MBC, PPMBC, and 79-PPMBC animals. (E) Quantification of the terminal phenotypes as determined by macroscopic and histological/immunohistochemical analysis; int, intestinal. (F) Quantification of the frequency of $Ki67^+$ cells in lymphoma sections from the indicated genotypes. Each data point represents a lesion from an individual animal. (G-I) BCR sequencing was performed on cDNA of lesions histologically characterized as tumors and PNA^+ GCB cells from wildtype animals. (G) shows representative clonality plots of 1 sample per genotype. Within each sample, each circle represents a unique BCR sequence, whereas the size of the circle represents the frequency of this sequence within the sample. Sequences differing by a maximum of 2 nucleotides are considered to be clonally related and therefore connected to clones by connecting lines. The dominant clone of

enrichment of centrocyte and MB features in PPMBC/79-PPMBC lymphomas and plasmacellular features in MBC/79-MBC tumors (supplemental Figure 2C). As we previously described for PPMBC lymphomas,[34] the combined presence of light-zone GC and MB features in the absence of transcriptome features associated with PB/plasma cell (PC) differentiation is consistent with malignant transformation of PPMBC and 79-PPMBC B cells occurring before PB differentiation at an intermediate stage between GC exit and MB cell differentiation. In line with a phenotype more closely related to the GC reaction, we found significantly higher *Aicda* expression levels in PPMBC and 79-PPMBC lymphomas than in MBC and 79-MBC cases, which display transcriptome features associated with a post-GC developmental stage (supplemental Figure 2D).

To further corroborate these transcriptome-based analyses, we next performed flow cytometry experiments to compare the relative abundance of MB cells, GC B cells, as well as dark-zone and light-zone B cells in wildtype spleens and 79-PPMBC lymphoma–infiltrated spleens. Three of 9 lymphomas were $CD38^{+}/FAS^{-}/IgD^{-}$, in line with an MB cell phenotype, whereas 6 of 9 cases were $CD38^{+}/FAS^{+}/IgD^{-}$, consistent with an intermediate stage between GC B cells and MB cells (Figure 2C and supplemental Figure 2E). At the same time, these 79-PPMBC lymphomas stained largely $CXCR4^{-}/CD86^{+}$, consistent with a light-zone phenotype (Figure 2C and supplemental Figure 2F). In order to independently assess the prevalence of a potential MB cell phenotype across our genotypes, we used the murine (m) version of the widely recognized Microenvironment Cell Populations counter (MCP-counter and mMCP-counter),[35,36] using our bulk RNA-sequencing data. To determine the abundance of MB cells, a population defined by Petitprez et al[36] based on flow cytometry markers $CD19^{+}/B220^{+}/CD38^{+}/CD80^{+}/IgD^{lo}$ and their RNA-correlates, we compared the mMCP-counter scores. Our findings revealed a significantly higher score of MB cells in 79-PPMBC and PPMBC than in their MBC and 79-MBC counterparts (Figure 2D). Altogether, these data suggest a model in which malignant 79-PPMBC cells are not arrested at 1 precisely defined B-cell developmental stage but rather retain the ability to dynamically cycle between GC B and MB stages, whereas the path to terminal differentiation toward the PB/PC stage is blocked. In line with such a model, 79-PPMBC–derived lymphomas clearly display transcriptomic features of pre-MB as well as light-zone B cells (Figure 2B and supplemental Figure 2B), while not showing any PB differentiation features, including a consistent lack of CD138 expression (Figures 1D, 2B, and supplemental Figure 2B). In contrast, MBC and 79-MBC cases clearly demonstrate CD138 positivity as an indicator of PB differentiation, while simultaneously displaying transcriptomic features still mapping to light-zone B cells (Figures 1D, 2B, and supplemental Figure 2B).

Myd88 and *Cd79b* comutant murine lymphomas display genetic features reminiscent of human ABC-DLBCL

Given the long latency to lymphoma development even in the 79-PPMBC model (median, 37.4 weeks; Figure 1B), and considering that human DLBCL cases harbor an average of 17 distinct genetic driver events,[6] we asked whether our DLBCL models acquired additional recurrent somatic mutations during lymphomagenesis. Thus, we next performed whole-exome sequencing (WES) on MBC (n = 16), 79-MBC (n = 17), PPMBC (n = 18), and 79-PPMBC (n = 14) lymphomas derived from individual mice. Next to a series of recurrent somatic copy number aberrations involving, among others, gains affecting *Myc* and losses involving *Trp73* (supplemental Figure 3A), this analysis returned recurrent abberations in *Pim1*, *Etv6*, *Irf2bp2*, *Bcl2*, *Nfkbia*, *Fas*, *Myc*, *Kmt2d* and other genes, which are recurrently mutated in DLBCL in general and the MCD/C5 cluster in particular[6,7] (Fig. 2E). A further analysis revealed that the 4 lymphoma genotypes were individually enriched for additional somatic mutations, possibly indicating that the engineered genetic makeups of each individual lymphoma model generate distinct molecular liabilities and dependencies, which, in turn, may necessitate distinct additional genomic aberrations during the course of multistep lymphomagenesis. We note that particularly the 79-PPMBC model was enriched for spontaneous somatic mutations associated with human MCD/C5 cases, such as *Pim1* (MCD, 92.5%), *Pim2* (MCD, 25.0%), *Mpeg1* (MCD, 43.8%), and *Etv6* (MCD, 55.0%), and genes that are frequently altered in MCD/C5, despite not being specifically associated with that cluster, such as *Irf2bp2* (MCD, 21.2%; *N*1, 43.8%) and *Ciita* (MCD, 7.5%; EZB, 25.0%),[9] further indicating that this model closely resembles the human scenario (Figure 2E). Moreover, 79-PPMBC cases harbored some of the highest tumor mutational burdens among all 4 models (Figure 2E).

We next performed an additional overrepresentation analysis, using enrichr. However, this time, we included genes that were recurrently mutated for each individual genotype to evaluate our observation regarding the enrichment of genes frequently mutated in MCD/C5 DLBCL. Through this analysis, we discovered that the recurrently mutated genes in our 79-PPMBC genotype were significantly associated with "B-cell activation" and "DLBCL ABC subtype," among other factors (supplemental Figure 3B). Furthermore, these genes ranked first in terms of the highest overlap. Interestingly, the PPMBC genotype also displayed a significant enrichment for similar terms, albeit with a lower gene overlap, resulting in a lower rank. Thus, altogether, our WES data provide further cross-species validation of our models and particularly position the 79-PPMBC model as a faithful preclinical avatar of human MCD/C5 lymphomas.

Cd79b-mutant murine lymphomas display an enhanced and actionable BCR signaling output

We had previously shown that PPMBC lymphomas display increased BCR signaling, compared with MBC cases, likely due to a developmental arrest before the PB stage, in which B cells still express surface BCRs.[18] Here, we used phospho-flow cytometry to ask whether engineering a B-cell–specific *Cd79b* ITAM mutation onto the MBC and PPMBC backgrounds results in enhanced BCR signaling output. As shown in Figure 3A-B, both freshly isolated 79-MBC and 79-PPMBC lymphoma cells displayed significantly increased phospho-PLCγ2 and phospho-SYK, compared to MBC and PPMBC control samples, indicating that the *Cd79b*

Figure 1 (continued) each sample is highlighted in blue. The size of the largest clone of each analyzed sample (PNA^{+} B, n = 4; MBC, n = 8; 79-MBC, n = 10; PPMBC, n = 5; and 79-PPMBC, n = 6) is plotted in panel H and the identified heavy chains are quantified in panel I; $^{*}P \leq .05$; Welch 2-tailed *t* test, Benjamini-Hochberg-correction for multihypothesis testing. cDNA, complementary DNA; PNA, peanut agglutinin.

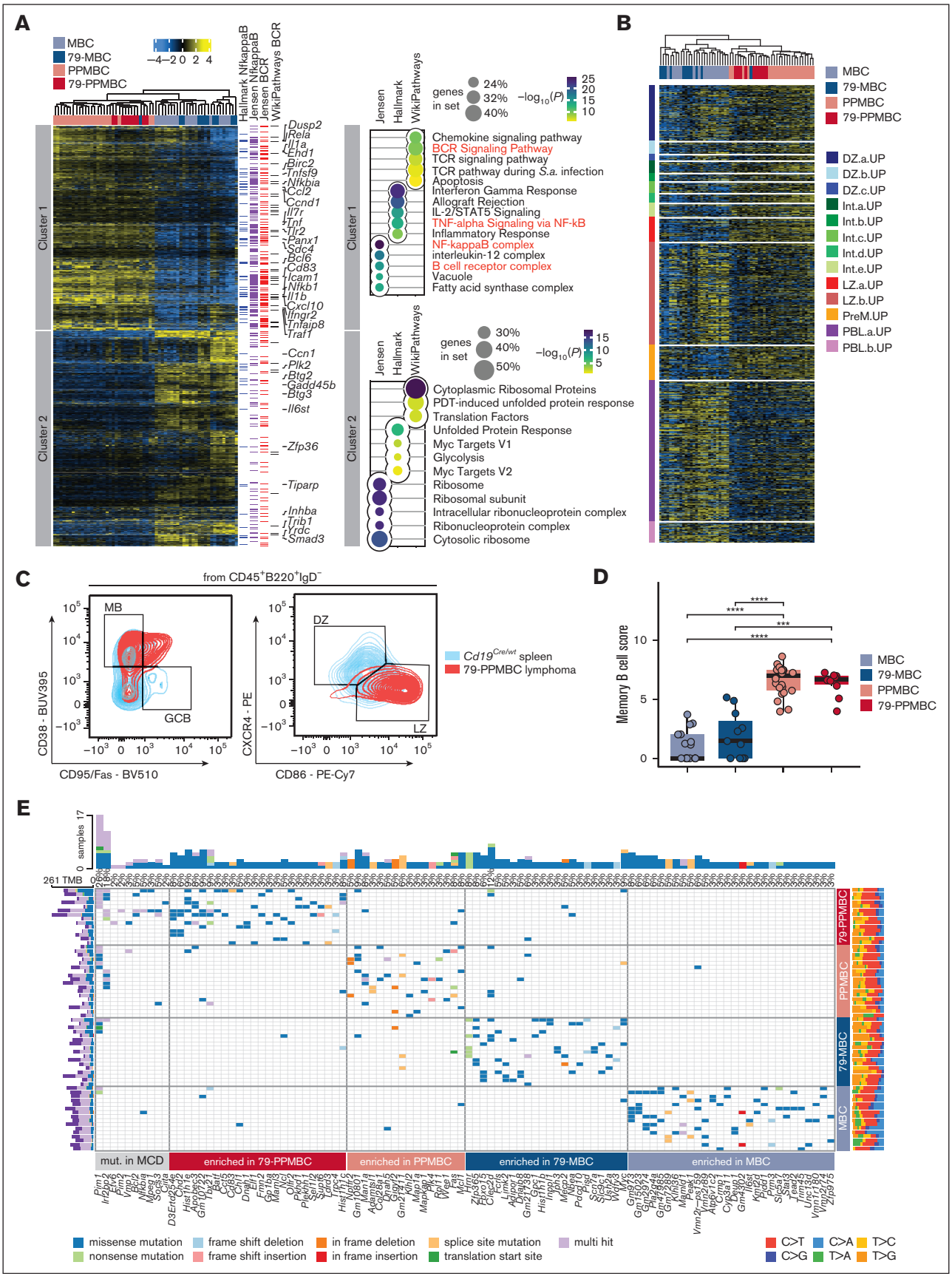

Figure 2.

p.Y195H mutation promotes BCR signaling output. Moreover, using proximity ligation assays (PLA) on lymphoma sections, we found a significantly increased complex formation between MYD88 and CD79B, as well as between MYD88 and MALT1, and MYD88 and BTK in the *Cd79b*-mutant models, compared to the parental MBC and PPMBC lymphomas (Figures 3C-E and supplemental Figure 4A-C). Of note, when specific antibodies against MYD88, CD79B, BTK, or MALT1 were paired with isotype control antibodies, signal intensities were diminished, validating the specificity of the assay (supplemental Figure 4D). Z stacking showed PLA puncta to be localized outside the nucleus (supplemental Movies 1-3). This observation is in line with a previous report describing the so-called My-T-BCR complex, consisting of MYD88, TLR9, and the BCR, which was demonstrated to coordinate oncogenic NF-κB signaling in a subset of ibrutinib-sensitive ABC-DLBCL cases.[37]

Next, we treated lymphoma-bearing MBC, 79-MBC, PPMBC, and 79-PPMBC animals with ibrutinib (30 mg/kg orally, daily p.o., q.d. on days 1-3) and assessed MYD88:CD79B, MYD88:MALT1, and MYD88:BTK complex formations as a function of ibrutinib exposure. These experiments showed that acute ibrutinib treatment disrupted all 3 complexes in 79-MBC and 79-PPMBC and returned the PLA signal to baseline levels comparable with those observed in MBC and PPMBC lymphomas (Figures 3C-E and supplemental Figure 4A-C).

Building on the selective ibrutinib-mediated disruption of MYD88:CD79B, MYD88:MALT1, and MYD88:BTK complexes, specifically in lymphomas harboring combined oncogenic *Myd88* and *Cd79b* mutations, we next asked whether these lymphomas derived enhanced therapeutic benefit from ibrutinib, compared with *Cd79b* wildtype lymphomas. To this end, we generated cohorts of MBC, 79-MBC, PPMBC, and 79-PPMBC animals. Lymphoma development was monitored by serial MRI scanning (Figure 4A). Upon overt lymphoma manifestation, ibrutinib treatment was initiated and tumor volumes were assessed through weekly MRI monitoring (Figure 4A, B). Ibrutinib did not induce any substantial lymphoma regression in MBC animals, whereas PPMBC animals displayed MRI-morphological responses, which also translated into significantly increased progression-free survival and OS (Figure 4A-D). This is in line with the significantly higher expression of genes associated with the BCR signaling pathway that we observed in our comparative transcriptomics analysis (Figure 2A-B and supplemental Figure 2B). More importantly, 79-MBC lymphoma–bearing animals displayed substantial MRI-assessed lymphoma regressions and derived significant progression-free survival and OS benefits from ibrutinib treatment, compared with MBC mice (Figure 4A-D). This effect of *Cd79b* p.Y195H mutation was even more pronounced in the 79-PPMBC setting than in PPMBC animals (Figure 4A-D). Thus, altogether, murine lymphomas harboring oncogenic *Myd88* and *Cd79b* mutations display exquisite sensitivity against single-agent ibrutinib. This observation is also in line with a recently conducted open-label, nonrandomized, prospective phase 1/2 analysis of ibrutinib in R/R DLBCL.[38]

Nevertheless, despite the initial remissions observed in 79-MBC and 79-PPMBC lymphomas, disease inevitably relapsed under continued ibrutinib exposure and led to the demise of the animals (Figure 4D). To gather a glimpse at potential mechanisms of drug resistance in this setting, we performed WES on 9 relapsed and 31 ibrutinib-naïve 79-PPMBC–derived lymphomas (supplemental Figure 4E). In these experiments, we did not detect recurrent mutations in genes that are known to drive ibrutinib resistance in human lymphomas, such as *Btk* or *Plcg2*. Functionally, however, we note that both 79-MBC and 79-PPMBC lymphomas displayed at least partially restored MYD88:CD79B PLA puncta upon overt preclinical resistance manifestation under ongoing ibrutinib exposure (Figure 4E-F). In summary, these data suggest that phenotypical ibrutinib resistance may require restoration of signaling complexes associated with downstream NF-κB signaling.

Discussion

Here, we generated a series of *Myd88*/*Cd79b* mutant autochthonous murine DLBCL models (summarized in supplemental Table 1). Using a 79-PPMB-$Cd21^{Cre/wt}$ setup, we recently showed that in a premalignant state, these animals displayed a spontaneous expansion of splenic GCs.[39] Moreover, 79-PPMB-$Cd21^{Cre/wt}$ splenic GC B cells showed supraphysiological proliferation and enhanced expression of IRF4. Of note, 5 of 8 79-PPMB-$Aicda^{Cre/wt}$ mice developed splenic tumors that displayed morphological features of DLBCL and were dominated by clonal B cells.[39] Building on these data largely derived from the premalignant setting, we, here, set out to characterize the lymphomas that develop in the 79-MBC and 79-PPMBC settings, as well as assess aberrant BCR signaling in these tumors.

Figure 2. *Myd88*-driven mouse models display genomic and transcriptomic features reminiscent of human ABC-DLBCL. (A) A heat map was generated from genes expressed differentially between the individual pairs of genotypes. The normalized DeSeq2 counts were centered after a row-wise mean subtraction. Highlighted MGI Gene Symbols were extracted from the Hallmark NfkappaB signature, Jensen compartments of NfkappaB, Jensen B-cell receptor (BCR) complex, and WikiPathways BCR, which were also significantly enriched in cluster 1. The right panel shows dot plots of significantly altered gene sets within cluster 1 and cluster 2, respectively. The size of the dot corresponds to the number of genes overlapping between the given cluster and the gene set, whereas the adjusted *P* value is visualized following a color code with an individual legend being provided. Gene sets highlighted in the heat map are marked in red color (n = 60). (B) Murine lymphoma transcriptomes were clustered by the expression of genes included in a published set of gene signatures specific to different GC developmental stages; DZ, dark zone; Int, intermediate; LZ, light zone; PreM, prememory; PBL, plasmablast. (C) Flow cytometric analyses of lymphoma samples for the expression of memory ($CD38^+/Fas^-$, gate "MB") and germinal center B cell ($CD38^-/Fas^+$, gate "GCB") surface markers. The expression levels of CXCR4 and CD86 were determined to distinguish between light and dark zone profiles (gates "LZ" and "DZ"). Splenocytes from $Cd19^{Cre/wt}$ were used as a reference. One case representative of 9 analyzed 79-PPMBC tumors is illustrated, the full set of cases is visualized in supplemental Figure 2E-F. (D) The abundance of memory B cells across different genotypes was quantitatively estimated using mMCP-counter, a method that uses a proprietary score to estimate the abundance of specific cell types (n = 60). (E) Oncoplot from MBC, 79-MBC, PPMBC, and 79-PMBC lymphomas (n = 65). Displayed are recurrently mutated genes identified using OncodriveCLUST,[29] a method specifically designed to identify significantly mutated genes that are subject to positive selection in cancer. These genes have been implicated in MCD DLBCL, as indicated by the "mut. in MCD" label. Moreover, mutations that are significantly enriched in any of the investigated genotypes are depicted. IL-2, interleukin 2; PDT, photodynamic therapy; TNF, tumor necrosis factor.

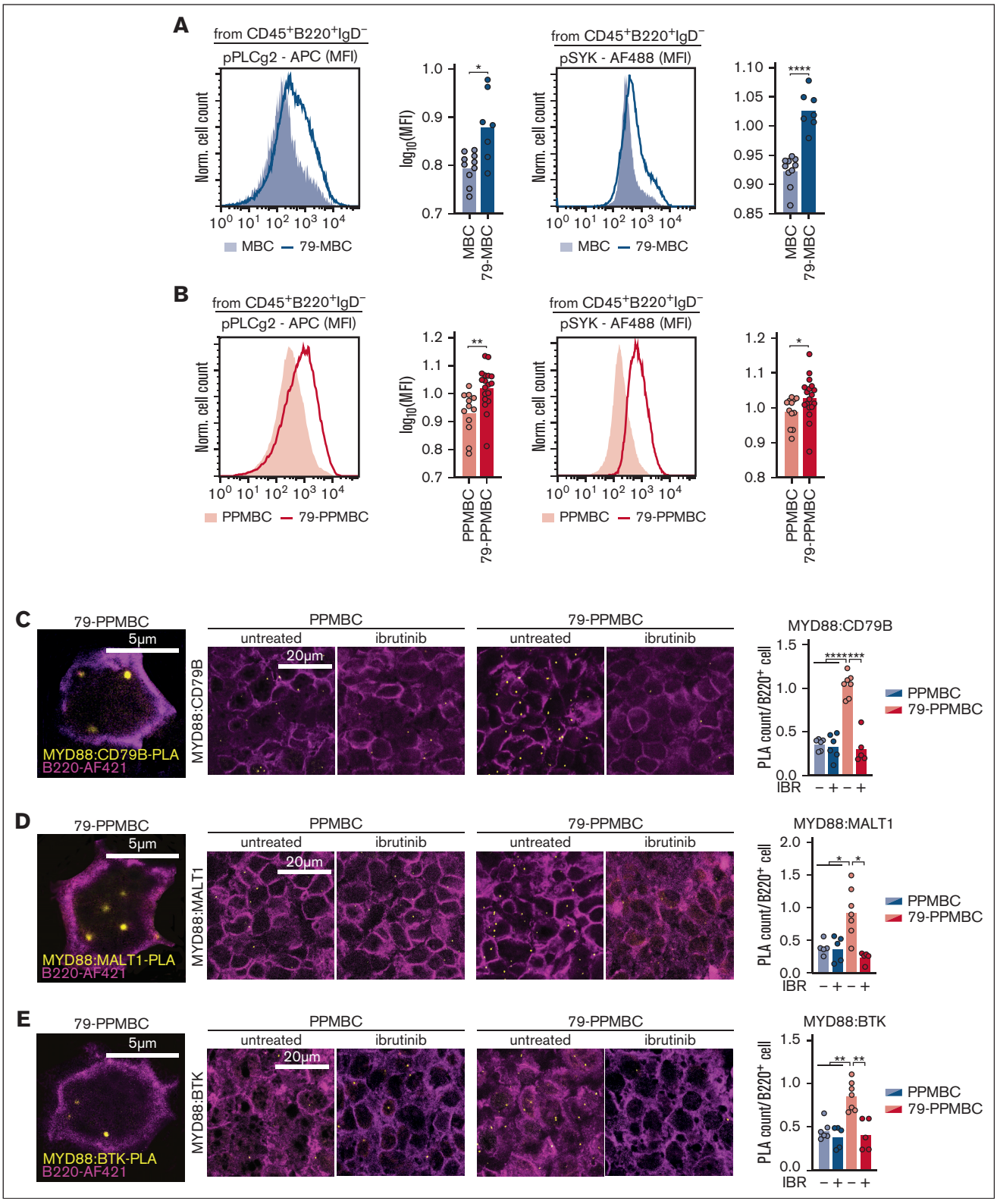

Figure 3. *Cd79b* p.Y195H augments BCR signaling. (A) Lymphoma cells of MBC and 79-MBC lymphomas were analyzed for levels of phosphorylated PLCg2 and SYK by flow cytometry. Representative cases are visualized as histograms, the geometric mean fluorescence intensity (MFI) is quantified for all analyzed cases (MBC, n = 10; and 79-MBC, n = 7). (B) The levels of phosphorylated PLCg2 and SYK in PPMBC and 79-PPMBC lymphoma cells were determined by flow cytometry. Visualized are representative cases; the MFIs of 12 PPMBC and 18 79-PPMBC lymphoma samples were quantified. (C) PLAs to detect the proximity of MYD88 and CD79B were performed on FFPE samples of PPMBC and 79-PPMBC lymphomas. Before sample collection, the animals were either left untreated or treated acutely with ibrutinib (30mg/kg orally, daily for 3 days). PLA foci

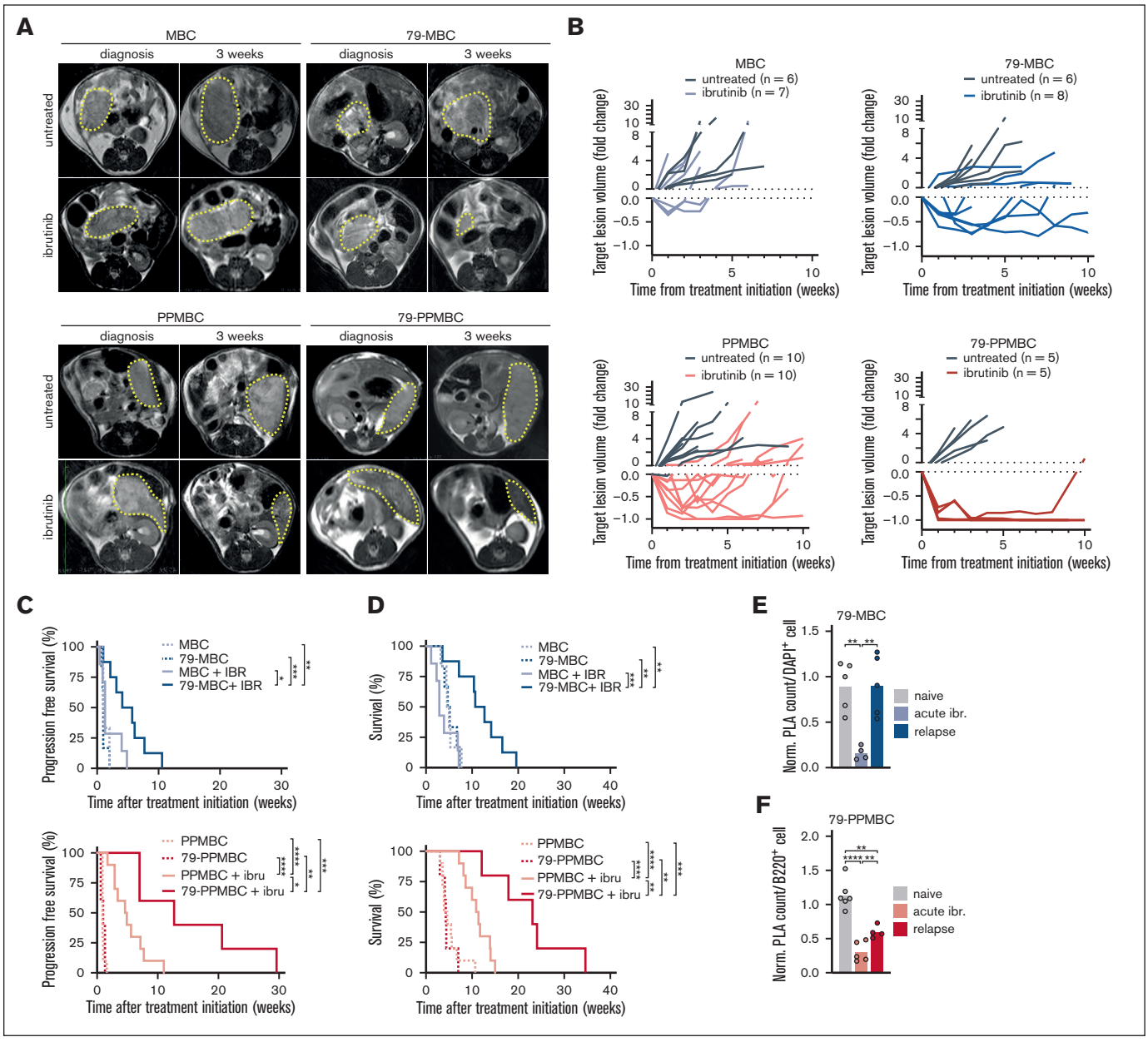

Figure 4. *Cd79b* p.Y195H confers ibrutinib sensitivity in vivo. MBC, 79-MBC, PPMBC, and 79-PPMBC mice were monitored for lymphoma development by MRI and upon tumor diagnosis either left untreated or treated with ibrutinib. (A) MRI images illustrate a baseline scan and after 3 weeks of ibrutinib treatment for a representative animal of each genotype and cohort. (B) Volume changes of target lesions over time are visualized for all 4 genotypes. Progression-free survival (C) and OS (D) is illustrated . (E), (F) PLA detecting the proximity of MYD88 and CD79B was done on FFPE tissue sections of ibrutinib relapsed 79-MBC and 79-PPMBC lymphomas and compared with PLA counts of treatment-naïve lesions of the same genotype, as well as tumor samples isolated from acutely treated animals (30 mg/kg orally daily for 3 days). *$P \leq .05$, **$P \leq .01$, ***$P \leq .001$, ****$P \leq .0001$; (C-D) Log-rank test. (E-F) Welch 2-tailed *t* test, corrected for multihypothesis testing (Benjamini-Hochberg).

Although engineering the *Cd79b* p.Y195H mutation into the MBC and PPMBC models did not produce a substantial disease acceleration (Figure 1A-F), we observed a remarkable shift from primarily IgG surface BCRs in PPMBC lymphomas toward IgM BCRs in the 79-PPMBC tumors (Figure 1I). Human ABC-DLBCLs frequently express an IgM BCR, whereas GCB DLBCLs typically display IgG BCRs.[28] In line with this observation, our 79-PPMBC–derived lymphomas were largely IgM

Figure 3 (continued) are visualized in yellow, and B220 staining (violet) was used to determine cell numbers. The PLA count per cell was quantified for a minimum of 5 independent lymphomas per condition. PLAs were performed in a similar manner to detect the proximity of MYD88 with MALT1 (D) and BTK (E). *$P \leq .05$, **$P \leq .01$, ***$P \leq .001$, ****$P \leq .0001$. Welch's 2-tailed *t* test, Benjamini-Hochberg-correction for multihypothesis testing. APC, allophycocyanin; FFPE, formalin-fixed, paraffin-embedded.

positive (Figure 1I). This is relevant because IgM and IgG BCRs drive qualitatively distinct intracellular signaling outputs.[3] Although membrane-bound IgM only displays 2 intracellular amino acid residues and thus largely hinges on CD79A and B to mediate intracellular signal transduction, IgG carries a long cytoplasmic C terminus, which contains a PDZ-domain–binding site, as well as a tyrosine phosphorylation site.[3] Based on these differences, it is perhaps not surprising that IgG BCRs relay potent MAPK and calcium release signaling, which promote B-cell differentiation toward plasma cells.[3] The signaling output mediated by IgM BCRs predominately consists of mitogenic signals that are less effective in promoting B-cell differentiation. This may rationalize why ABC-DLBCLs are selected to retain IgM BCR signaling, because this sustains proliferation and survival rather than driving terminal PB/PC differentiation.

We noted no significant disease acceleration when introducing the *Cd79b*$^{c.\text{-}p.Y195H}$ allele onto the MBC and PPMBC backgrounds. This observation is in line with a recent report showing that the cytotoxic effect of RNAi-mediated *CD79B* depletion in the DLBCL cell line HBL1 (harboring a *CD79B* p.Y196F mutation) could be rescued by both, *CD79B* wildtype and various ITAM-mutant cDNAs.[21] Importantly, there was no quantitative difference in the ability to rescue the *CD79B* depletion phenotype between wildtype and mutant cDNAs, possibly indicating that *CD79B* ITAM mutants do not provide a proliferative advantage *per se*.[21] Based on this observation, it was proposed that the selection of *CD79B* ITAM mutations might be an early event during lymphomagenesis, enabling supraphysiological responses to self or foreign antigen.[3,21] Fittingly, it was shown that *Cd79a* and *Cd79b* ITAM aberrations in murine B cells promote enhanced antigen responses.[40-42] Nevertheless, given that *CD79B* mutations appear to be selected events in human DLBCL, it is somewhat surprising that 79-MBC and 79-PPMBC animals do not develop lymphomas earlier than their *Cd79b*-wildtype counterparts. However, it is important to note that in our *Cd19*^{Cre}-driven model system, *Cd79b* ITAM mutations are induced at the same time as *Myd88* and *BCL2* aberrations, which by themselves promote self-reactivity.[19] Altogether, this might mask an oncogenic effect of an early isolated *Cd79b* mutation.

Next to driving potent survival and proliferation signals, the BCR pathway also triggers negative feedback loops to restrict unlimited signaling. For instance, in murine B cells, it was demonstrated that mutations in the CD79B ITAM tyrosine residues increase surface BCR expression through the repression of receptor internalization.[40] In addition, a major negative-feedback loop is centered around LYN kinase, which on the 1 hand initiates BCR signaling by phosphorylating ITAM tyrosine residues and on the other hand, phosphorylates immunoreceptor tyrosine-based inhibitory motifs within the cytoplasmic tails of FcγRIIb or CD22.[3] Phosphorylated immunoreceptor tyrosine-based inhibitory motifs facilitate SHP1 recruitment, which catalyzes CD79B ITAM dephosphorylation and thus represses BCR signaling. Moreover, LYN kinase activity is reduced in *CD79B*-mutant cells compared with *CD79B* wildtype controls.[3,21,43] Thus, given that *CD79B* ITAM mutations appear to augment BCR signaling, the observation that BTK inhibition displayed selective toxicity in *Cd79b*-mutant 79-MBC and 79-PPMBC, compared with MBC and PPMBC lymphomas (Figure 4A-D), is perhaps not surprising.

Our WES analysis of 9 ibrutinib-exposed 79-PPMBC and 79-MBC lymphomas did not return *Btk* or *Plcg2* mutations that were shown to be associated with resistance against BTK inhibitors in patients with CLL.[44] This might be explained through alternative modes of resistance, including epigenetic mechanisms, as recently observed in ABC-DLBCL cell lines.[45]

Altogether, we consider our models preclinical avatars that can be used to study DLBCL biology and develop novel therapeutic strategies, which are urgently needed in the clinic.

Acknowledgments

The authors thank Alexandra Florin, Marion Müller, and Ursula Rommerscheidt-Fuß from the Institute of Pathology, University Hospital Cologne, for their outstanding technical support. Flow cytometry analyses, microscopy, and image-analysis were performed in the FACS and Imaging Core Facility at the Max Planck Institute for Biology of Ageing, Cologne. We acknowledge support by the Open Access Publication Fund of the University of Duisburg-Essen.

This work was funded through the German-Israeli Foundation for Research and Development (I-65-412.20-2016 [H.C.R.]), the Deutsche Forschungsgemeinschaft (RE 2246/13-1, SFB1399-A01, SFB1430-A09, SFB1530-A01 [H.C.R.] and PE3140/1-1 [B.P.]), the Else Kröner-Fresenius-Stiftung (EKFS-2014-A06 [H.C.R.] and 2016_Kolleg.19 [H.C.R. and R.D.J.]), the Deutsche Krebshilfe (1117240, 70113041, and an Excellence Funding Program Grant [H.C.R.]) and a Deutsche Krebshilfe Mildred Scheel Nachwuchszentrum Grant (grant number 70113307), the ERA-PerMed program HiRisk-HiGain (H.C.R.), as well as the German Ministry of Education and Research (BMBF e:Med 01ZX1303A [H.C.R.]). J.H. is member of the Cologne Graduate School of Ageing Research.

Authorship

Contribution: R.F., J.H., P.P., H.G.W., A.L., J.W., M.M., T.Z., A.T., T.L., M.J., S.H., A. A., and G.K. conducted experiments and collected the data; R.F., J.H., J.M., P.P., T.L., F.B., B.P., F.U., B.v.T., S.K., and G.K. performed analyses; R.F., J.H., S.K., R.D.J, H.C.R., and G.K. conceived and designed experiments; T.P. and R.B. contributed data; B.P., T.P., and R.B. contributed analysis tools; R.F., J.H., B.v.T., S.K., R.D.J., H.C.R., and G.K. wrote the manuscript.

Conflict-of-interest disclosure: H.C.R. received consulting and lecture fees from AbbVie, AstraZeneca, Roche, Janssen-Cilag, Novartis, Vertex, and Merck; research funding from Gilead and AstraZeneca; and is a cofounder of CDL Therapeutics GmbH. B.v.T. is an adviser or consultant for Allogene, BMS/Celgene, Cerus, Incyte, IQVIA, Gilead Kite, Miltenyi, Novartis, Noscendo, Pentixapharm, Roche, Amgen, Pfizer, Takeda, Merck Sharp & Dohme, and Gilead Kite; has received honoraria from AstraZeneca, BMS, Incyte, Novartis, Roche Pharma AG, Takeda, and Merck Sharp & Dohme; reports research funding from Novartis (institutional), Merck Sharp & Dohme (institutional), and Takeda (institutional); and travel support from AbbVie, AstraZeneca, Gilead Kite, Merck Sharp & Dohme, Roche, Takeda, and Novartis. The remaining authors declare no competing financial interests.

ORCID profiles: J.H., 0000-0001-7828-1269; J.W., 0009-0000-1994-1722; T.L., 0000-0002-3216-0784; B.P., 0000-0002-1892-3650; F.U., 0000-0002-5033-2201; A.A., 0000-0002-2789-2593; R.B., 0000-0001-8806-4786; B.v.T., 0000-0003-1410-

4487; S.K., 0000-0002-2188-9377; R.D.J., 0000-0001-9522-7061; G.K., 0000-0001-8395-3701.

Correspondence: H. C. Reinhardt, University Hospital Essen, Department of Hematology and Stem Cell Transplantation, West German Cancer Center, German Cancer Consortium Partner Site Essen, Center for Molecular Biotechnology, University of Duisburg-Essen, Hufelandstraße 55 45147, Essen, Germany; email: christian.reinhardt@uk-essen.de; and G. Knittel; email: gero.knittel@uk-essen.de.

References

1. Swerdlow SH, Campo E, Pileri SA, et al. The 2016 revision of the World Health Organization classification of lymphoid neoplasms. *Blood*. 2016;127(20):2375-2390.
2. Alizadeh AA, Eisen MB, Davis RE, et al. Distinct types of diffuse large B-cell lymphoma identified by gene expression profiling. *Nature*. 2000;403(6769):503-511.
3. Shaffer AL 3rd, Young RM, Staudt LM. Pathogenesis of human B cell lymphomas. *Annu Rev Immunol*. 2012;30:565-610.
4. Lenz G, Wright G, Dave SS, et al. Stromal gene signatures in large-B-cell lymphomas. *N Engl J Med*. 2008;359(22):2313-2323.
5. Rosenwald A, Wright G, Chan WC, et al. The use of molecular profiling to predict survival after chemotherapy for diffuse large-B-cell lymphoma. *N Engl J Med*. 2002;346(25):1937-1947.
6. Chapuy B, Stewart C, Dunford AJ, et al. Molecular subtypes of diffuse large B cell lymphoma are associated with distinct pathogenic mechanisms and outcomes. *Nat Med*. 2018;24(5):679-690.
7. Schmitz R, Wright GW, Huang DW, et al. Genetics and pathogenesis of diffuse large B-cell lymphoma. *N Engl J Med*. 2018;378(15):1396-1407.
8. Lacy SE, Barrans SL, Beer PA, et al. Targeted sequencing in DLBCL, molecular subtypes, and outcomes: a Haematological Malignancy Research Network report. *Blood*. 2020;135(20):1759-1771.
9. Wright GW, Huang DW, Phelan JD, et al. A probabilistic classification tool for genetic subtypes of diffuse large B cell lymphoma with therapeutic implications. *Cancer Cell*. 2020;37(4):551-568.e14.
10. Pfreundschuh M, Kuhnt E, Trümper L, et al. CHOP-like chemotherapy with or without rituximab in young patients with good-prognosis diffuse large-B-cell lymphoma: 6-year results of an open-label randomised study of the MabThera International Trial (MInT) Group. *Lancet Oncol*. 2011;12(11):1013-1022.
11. Pfreundschuh M, Schubert J, Ziepert M, et al. Six versus eight cycles of bi-weekly CHOP-14 with or without rituximab in elderly patients with aggressive CD20+ B-cell lymphomas: a randomised controlled trial (RICOVER-60). *Lancet Oncol*. 2008;9(2):105-116.
12. Dickinson MJ, Carlo-Stella C, Morschhauser F, et al. Glofitamab for relapsed or refractory diffuse large B-cell lymphoma. *N Engl J Med*. 2022;387(24):2220-2231.
13. Gisselbrecht C, Glass B, Mounier N, et al. Salvage regimens with autologous transplantation for relapsed large B-cell lymphoma in the rituximab era. *J Clin Oncol*. 2010;28(27):4184-4190.
14. Horwitz SM, Negrin RS, Blume KG, et al. Rituximab as adjuvant to high-dose therapy and autologous hematopoietic cell transplantation for aggressive non-Hodgkin lymphoma. *Blood*. 2004;103(3):777-783.
15. Kewalramani T, Zelenetz AD, Nimer SD, et al. Rituximab and ICE as second-line therapy before autologous stem cell transplantation for relapsed or primary refractory diffuse large B-cell lymphoma. *Blood*. 2004;103(10):3684-3688.
16. Tilly H, Gomes da Silva M, Vitolo U, et al. Diffuse large B-cell lymphoma (DLBCL): ESMO Clinical Practice Guidelines for diagnosis, treatment and follow-up. *Ann Oncol*. 2015;26(suppl 5):v116-125.
17. Chow VA, Shadman M, Gopal AK. Translating anti-CD19 CAR T-cell therapy into clinical practice for relapsed/refractory diffuse large B-cell lymphoma. *Blood*. 2018;132(8):777-781.
18. Flümann R, Hansen J, Pelzer BW, et al. Distinct genetically determined origins of Myd88/BCL2-driven aggressive lymphoma rationalize targeted therapeutic intervention strategies. *Blood Cancer Discov*. 2023;4(1):78-97.
19. Flümann R, Rehkämper T, Nieper P, et al. An autochthonous mouse model of Myd88- and BCL2-driven diffuse large B-cell lymphoma reveals actionable molecular vulnerabilities. *Blood Cancer Discov*. 2021;2(1):70-91.
20. Knittel G, Liedgens P, Korovkina D, et al. B cell-specific conditional expression of Myd88p.L252P leads to the development of diffuse large B cell lymphoma in mice. *Blood*. 2016;127(22):2732-2741.
21. Davis RE, Ngo VN, Lenz G, et al. Chronic active B-cell-receptor signalling in diffuse large B-cell lymphoma. *Nature*. 2010;463(7277):88-92.
22. Shapiro-Shelef M, Lin KI, Savitsky D, Liao J, Calame K. Blimp-1 is required for maintenance of long-lived plasma cells in the bone marrow. *J Exp Med*. 2005;202(11):1471-1476.
23. Rickert RC, Roes J, Rajewsky K. B lymphocyte-specific, Cre-mediated mutagenesis in mice. *Nucleic Acids Res*. 1997;25(6):1317-1318.
24. Woyach JA, Bojnik E, Ruppert AS, et al. Bruton's tyrosine kinase (BTK) function is important to the development and expansion of chronic lymphocytic leukemia (CLL). *Blood*. 2014;123(8):1207-1213.
25. Dietlein F, Kalb B, Jokic M, et al. A synergistic interaction between Chk1- and MK2 inhibitors in KRAS-mutant cancer. *Cell*. 2015;162(1):146-159.

26. Torgovnick A, Heger JM, Liaki V, et al. The Cdkn1a(SUPER) mouse as a tool to study p53-mediated tumor suppression. *Cell Rep*. 2018;25(4):1027-1039.e6.
27. Young RM, Wu T, Schmitz R, et al. Survival of human lymphoma cells requires B-cell receptor engagement by self-antigens. *Proc Natl Acad Sci U S A*. 2015;112(44):13447-13454.
28. Lenz G, Nagel I, Siebert R, et al. Aberrant immunoglobulin class switch recombination and switch translocations in activated B cell-like diffuse large B cell lymphoma. *J Exp Med*. 2007;204(3):633-643.
29. Tamborero D, Gonzalez-Perez A, Lopez-Bigas N. OncodriveCLUST: exploiting the positional clustering of somatic mutations to identify cancer genes. *Bioinformatics*. 2013;29(18):2238-2244.
30. Chen EY, Tan CM, Kou Y, et al. Enrichr: interactive and collaborative HTML5 gene list enrichment analysis tool. *BMC Bioinformatics*. 2013;14:128.
31. Binder JX, Pletscher-Frankild S, Tsafou K, et al. COMPARTMENTS: unification and visualization of protein subcellular localization evidence. *Database (Oxford)*. 2014;2014:bau012.
32. Liberzon A, Birger C, Thorvaldsdóttir H, Ghandi M, Mesirov JP, Tamayo P. The Molecular Signatures Database (MSigDB) hallmark gene set collection. *Cell Syst*. 2015;1(6):417-425.
33. Slenter DN, Kutmon M, Hanspers K, et al. WikiPathways: a multifaceted pathway database bridging metabolomics to other omics research. *Nucleic Acids Res*. 2018;46(D1):D661-D667.
34. Holmes AB, Corinaldesi C, Shen Q, et al. Single-cell analysis of germinal-center B cells informs on lymphoma cell of origin and outcome. *J Exp Med*. 2020;217(10):e20200483.
35. Becht E, Giraldo NA, Lacroix L, et al. Estimating the population abundance of tissue-infiltrating immune and stromal cell populations using gene expression. *Genome Biol*. 2016;17(1):218.
36. Petitprez F, Levy S, Sun CM, et al. The murine Microenvironment Cell Population counter method to estimate abundance of tissue-infiltrating immune and stromal cell populations in murine samples using gene expression. *Genome Med*. 2020;12(1):86.
37. Phelan JD, Young RM, Webster DE, et al. A multiprotein supercomplex controlling oncogenic signalling in lymphoma. *Nature*. 2018;560(7718):387-391.
38. Wilson WH, Young RM, Schmitz R, et al. Targeting B cell receptor signaling with ibrutinib in diffuse large B cell lymphoma. *Nat Med*. 2015;21(8):922-926.
39. Pindzola GM, Razzaghi R, Tavory RN, et al. Aberrant expansion of spontaneous splenic germinal centers induced by hallmark genetic lesions of aggressive lymphoma. *Blood*. 2022;140(10):1119-1131.
40. Gazumyan A, Reichlin A, Nussenzweig MC. Ig beta tyrosine residues contribute to the control of B cell receptor signaling by regulating receptor internalization. *J Exp Med*. 2006;203(7):1785-1794.
41. Kraus M, Saijo K, Torres RM, Rajewsky K. Ig-alpha cytoplasmic truncation renders immature B cells more sensitive to antigen contact. *Immunity*. 1999;11(5):537-545.
42. Torres RM, Hafen K. A negative regulatory role for Ig-alpha during B cell development. *Immunity*. 1999;11(5):527-536.
43. Xu Y, Harder KW, Huntington ND, Hibbs ML, Tarlinton DM. Lyn tyrosine kinase: accentuating the positive and the negative. *Immunity*. 2005;22(1):9-18.
44. Woyach JA, Furman RR, Liu TM, et al. Resistance mechanisms for the Bruton's tyrosine kinase inhibitor ibrutinib. *N Engl J Med*. 2014;370(24):2286-2294.
45. Shaffer AL 3rd, Phelan JD, Wang JQ, et al. Overcoming acquired epigenetic resistance to BTK inhibitors. *Blood Cancer Discov*. 2021;2(6):630-647.